PREDICTION, MEASUREMENT, AND SUPPRESSION OF HIGH TEMPERATURE SUPERSONIC JET NOISE

John M. Seiner and T.R.S. Bhat
Jet Noise Laboratory
NASA Langley Research Center
Hampton, Virginia

and

Bernard J. Jansen
Lockheed Engineering and Sciences Company
Hampton, Virginia

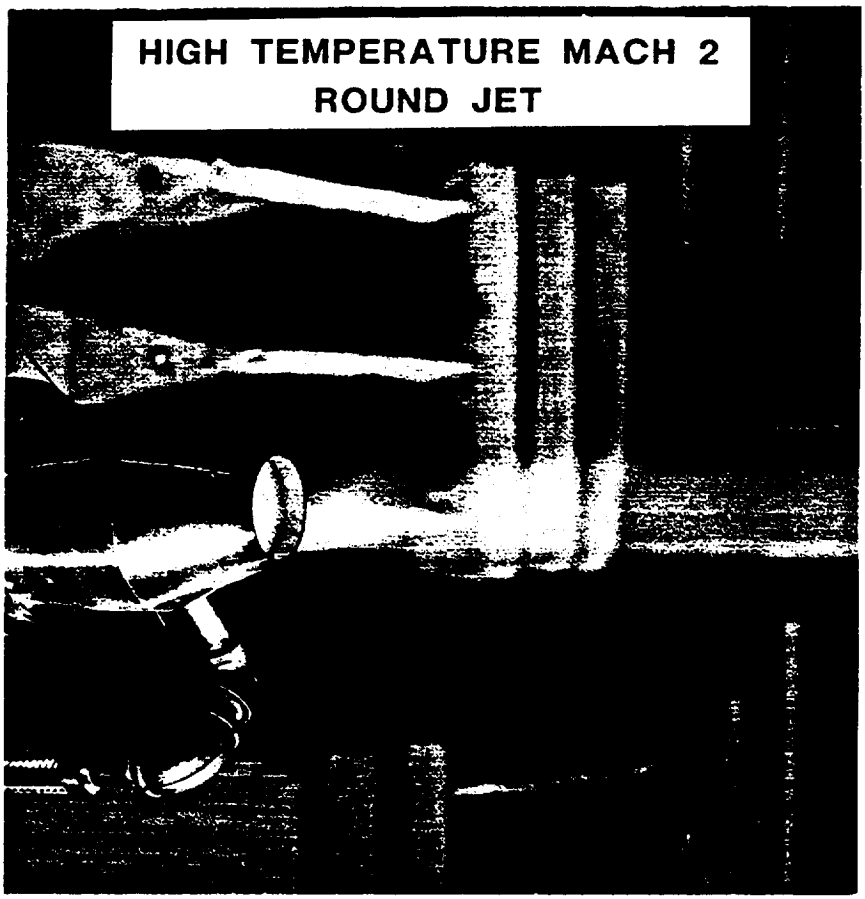

Figure 1

The photograph in figure 1 displays a water cooled round convergent-divergent supersonic nozzle operating slightly overexpanded near 2460°F. The nozzle is designed to produce shock free flow near this temperature at Mach 2. The exit diameter of this nozzle is 3.5 inches. This nozzle is used in the present study to establish properties of the sound field associated with high temperature supersonic jets operating fully pressure balanced (i.e. shock free) and to evaluate capability of the compressible Rayleigh model to account for principle physical features of the observed sound emission. The experiment is conducted statically (i.e. M_f = 0.) in the NASA/LaRC Jet Noise Laboratory. Both aerodynamic and acoustic measurements are obtained in this study along with numerical plume simulation and theoretical prediction of jet noise. Detailed results from this study are reported previously by Seiner, Ponton, Jansen, and Lagen (1992).

TAM AND OERTEL'S CONVECTIVE MACH NUMBER RELATIONS

I. Supersonic instability waves

$$M_c = V_c / C_A = (V_j - V_c) / C_j = V_j / (C_j + C_A)$$

II. Kelvin-Helmholtz instability waves (eddy Mach wave emission)

$$M_c' = V_c' / C_A = (V_j - V_c') / C_j + 1 = (V_j + C_j) / (C_j + C_A)$$

III. Subsonic instability waves

$$M_c'' = V_c'' / C_A = (V_j - V_c'') / C_j - 1 = (V_j - C_j) / (C_j + C_A)$$

Figure 2

In the early 1980's, Oertel (1982) observed the existence of three distinct families of waves in the shear layer of an unheated high Mach number supersonic jet generated by a shock tube. Using time resolved photographic renditions, Oertel distinguished one family of waves from another by observation of their different convection velocities. He noted that the first family of waves were convected supersonically relative the sum of the local jet and ambient sound speed. The second family was convected supersonically relative to the ambient sound speed. The third family was convected subsonically; its speed governed by the difference between the local jet and sound speeds. For hot jets, however, even this wave could eventually convect supersonically at extreme Mach and jet total temperatures. Oertel developed simple convective Mach number relations for these families of waves, as shown in figure 2. Here, V_c, V_j, c_j, c_a, represent the convection, local jet velocity, local jet sound speed, and ambient sound speed.

More recently in a benchmark paper, Tam (1989) demonstrated that Oertel's convective Mach number relations actually satisfied those obtained from solution of the compressible Rayleigh equation. The second family of waves were found to be associated with the familiar Kelvin-Helmholtz instability waves. The first family of waves were obtained by extension of the Rayleigh model to include radial modes. Both the first and second families of waves are expected to be important sources of noise emission because of their supersonic phase speed. The third family of waves are technically unimportant because of their subsonic phase speed in the range of both Mach and jet total temperatures typically encountered in aircraft jet engines being considered for the NASA HSR program.

DEFINITION OF MACH WAVE ANGLE

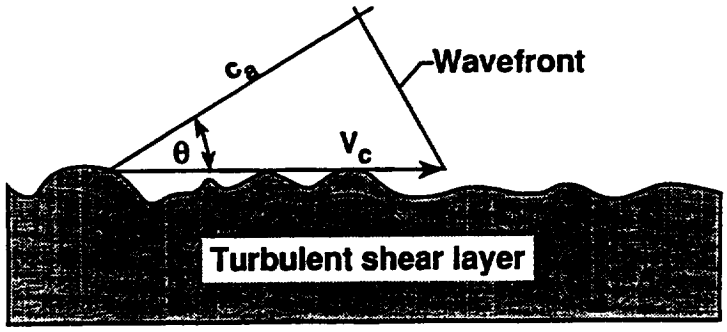

Figure 3

Figure 3 illustrates the convention used to define the Mach wave angle is shown in the figure. Here, V_c, is the convection velocity of turbulence in the jet shear layer and, c_a, is the ambient sound speed. The acoustic wavefront is propagated, as shown, at an angle, θ, to the turbulent shear layer.

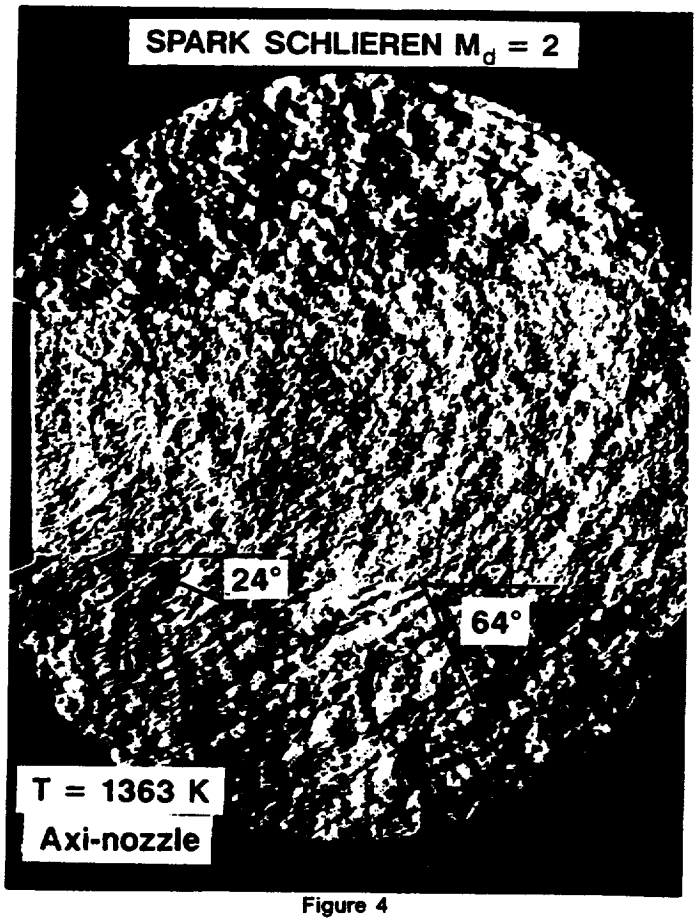

Figure 4

By way of illustration, consider the spark schlieren photograph of figure 4. This photographic record was obtained using M_d = 2 water cooled nozzle. The nozzle was operated overexpanded (i.e. M_j = 1.8) at 1370°K. This record, taken with a vertical knife edge and spark duration < 0.1 μ-sec., captures a nearly instantaneous view of both the flow and near acoustic field. The acoustic waves that emanate from along the edge of the jet shear layer are produced by turbulence convecting supersonically. For this Mach number and jet total temperature, one expects that both the first and second families of waves will have supersonic phase speeds based on the convective Mach number relations in figure 3.

The schlieren record shows the presence of at least three types of acoustic waves. The first set are waves with very short wavelength , located near the nozzle exit. A second set of low amplitude waves, with a wavelength of at least an order of magnitude greater than those centered at the nozzle exit, appear to be propagating at low angles to the jet shear layer. The 24° vector indicates a best guess estimate of their direction. The third set of waves have even longer wavelengths and are of significantly greater amplitude. These waves appear to be inclined at 64° to the jet axis as indicated on the figure. The axial wavelength appears to increase with increasing downstream distance.

MACH WAVE EMISSION ANGLE

MACH ANGLE : $\theta = \cos^{-1}(1 / M_c) = \cos^{-1}(C_A / \alpha V_j)$

$\theta_c = 28^\circ$ - SUPERSONIC INSTABILITY WAVE

$\theta_c \approx 24^\circ$ - SCHLIEREN RECORD

$\theta_c' = 56^\circ$ - KELVIN-HELMHOLTZ INSTABILITY

$\theta_c' \approx 64^\circ$ - SCHLIEREN RECORD

Figure 5

Mach waves are emitted from the supersonic shear layer at an angle, θ, that depends on the convection speed of turbulence in the jet shear layer. This is illustrated graphically in figure 3 and can be computed as shown in figure 5 as the inverse cosine of , $1/M_c$, the convection Mach number. As we have seen from figure 2, the convection Mach number for each wave family can be determined from Oertel's relationships or computed from the phase speed based on solution of the compressible Rayleigh equation. In figure 5, α, represents a compilation of those terms necessary to compute the convection velocity, V_c, using these relationships for each family of wave. It is important to note, however, that turbulence is a dispersive medium. Thus the convection velocity is dependent on the turbulence frequency and axial location away from the jet axis, and consequently $\alpha = \alpha(x,\omega)$. For purposes of illustration with the spark schlieren of figure 4, the jet exhaust velocity and temperature are used to calculate a value for α. This can only be expected to provide a nominal value for the convection Mach number and Mach emission angle.

As shown in figure 5, the nominal value for the Mach emission angles for the first two families of instability waves is reasonably close to that displayed in the figure 4 schlieren. Later it will be shown that instability wave analysis also predicts that supersonic instability waves dominate high frequency Mach wave emission and originate closer to the jet axis than do the Kelvin-Helmholtz instability waves.

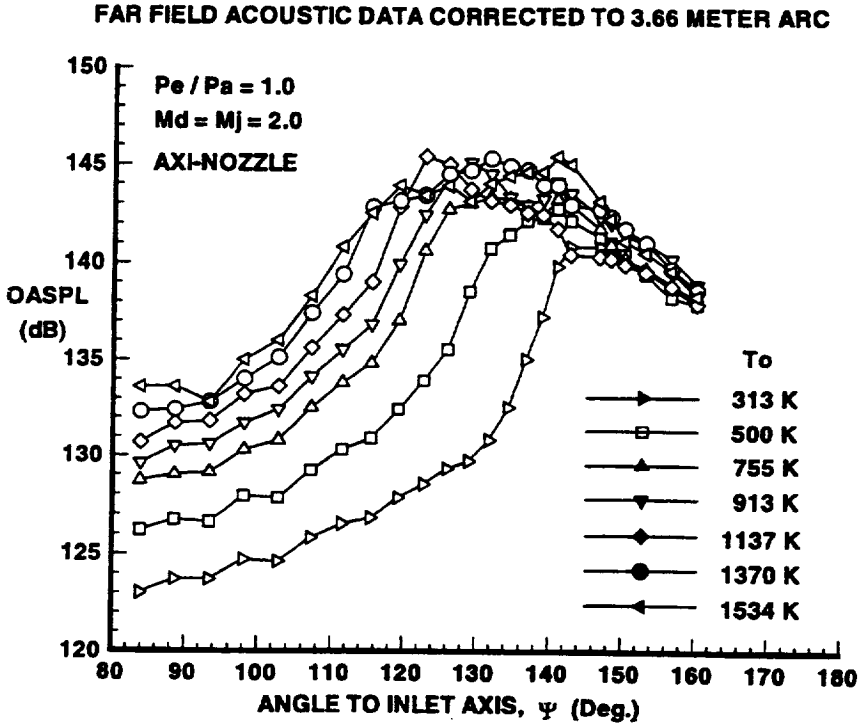

Figure 6

In figure 6, the overall sound pressure level (OASPL) in dB is shown for several jet total temperatures investigated using the M_d = 2 round nozzle. All results shown are for operation of the nozzle fully pressure balanced. The data is presented in terms of the angle to the nozzle inlet axis. The OASPL is computed from each microphone's digitized time record. The nozzle thrust is nearly constant for all temperature conditions. The relatively rapid rise in the OASPL from low temperatures to smaller increases at high temperature is expected, since the convective Mach number depends on the absolute jet temperature ratio T_j/T_a, where T_j, and T_a are respectively the jet total and ambient temperatures.

For each temperature there is a well defined peak amplitude region. The Mach wave emission process is confined to angles greater than ψ = 90°. At 313°K the peak OASPL lies near ψ_p = 145°. The angle, ψ_p, that defines other peak angles of emission, decreases with increasing jet temperature as expected form the convective Mach number relations of figure 2. At 1370°K, these convective Mach number relations predict that the supersonic instability waves would have the peak amplitude of emission occur at an angle of ψ = 143° and the K-H instability waves an angle of ψ = 122°. The 1370°K data of figure 6 show a major peak in OASPL near ψ_p = 129° and a minor peak near ψ_p = 137°. Thus reasonable agreement exist between the observed peak amplitude emission angles and those calculated nominal values.

NARROW BAND FAR FIELD ACOUSTIC SPECTRA
(M_j = 2.002, T_o = 1370°K)

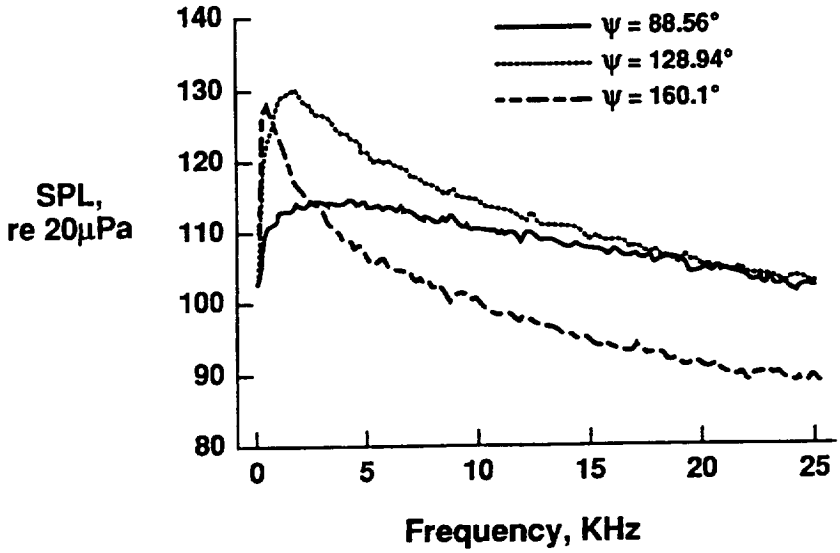

Figure 7

Several narrow band spectra at inlet angles of ψ = 88.9°, 128.9°, and 160.1° are shown in figure 7 for the T_j = 1370°K jet temperature condition. These spectra have been corrected to spectrum levels and only the first 25 kHz. of the 100 kHz. processed spectrum is shown to enhance details at low frequency.

The 88.6° spectrum lies outside the Mach wave emission field and is very flat without a well defined frequency of peak amplitude. The spectrum at the 128.9° shows a large increase in low frequency content with a well defined peak spectral value near 1.5 kHz. The spectrum at 160.1°, which lies well beyond the peak OASPL emission direction, indicates an even greater increase in low frequency emission with a very narrow band spectral peak. Very little high frequency noise is emitted in this direction, relative to the other two angles in figure 7.

DISTRIBUTION OF SPECTRUM PEAK AMPLITUDE LEVELS

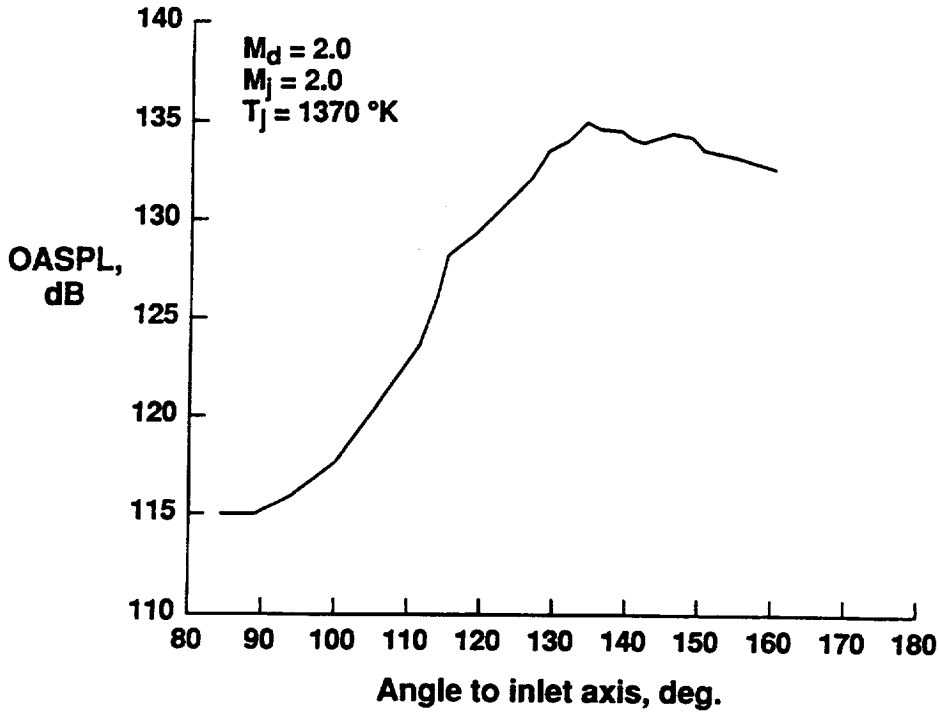

Figure 8

The angular distribution of spectral peak amplitude levels are shown in figure 8 for the jet total temperature of T_j = 1370°K. This data is generated from narrow band spectra like those of figure 7. The data of figure 8 indicates that the angular location, where the Mach wave emission process becomes important, lies between ψ = 100° and 110°. After reaching a peak value at ψ = 134°, the peak amplitude spectral values remain relatively constant with increasing angular position.

STROUHAL FREQUENCY TREND WITH ANGLE TO INLET AXIS

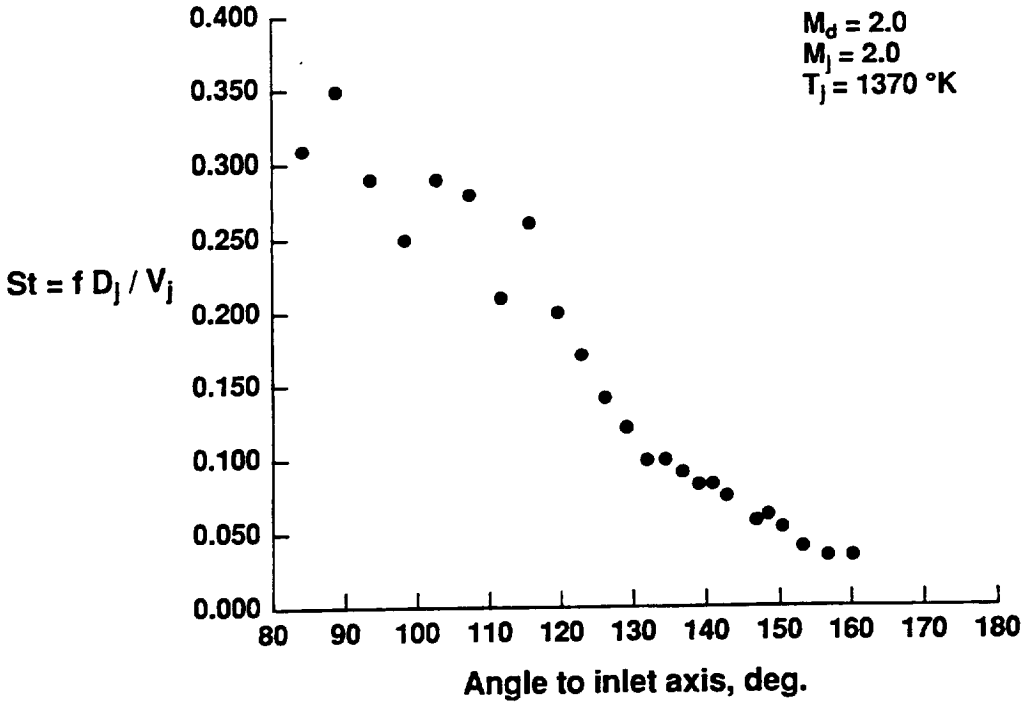

Figure 9

For the same jet operating, figure 9 shows the angular dependence of the frequency identifying the peak spectral amplitude. The data is presented in terms of the Strouhal frequency, S_t, where $S_t = fD/V_j$. The Strouhal frequency is seen to decrease from values near 0.35 at $\psi = 90°$ to values near 0.03 at $\psi = 160°$. The scatter in Strouhal frequencies at lower angles of ψ is due to limitation in identification of a spectrum peak amplitude from a flat spectrum, like that shown in the figure 7 spectrum for $\psi_p = 88.56^0$. The angular dependence of the Strouhal frequency and spectral peak amplitude are important characteristics of the Mach wave emission process.

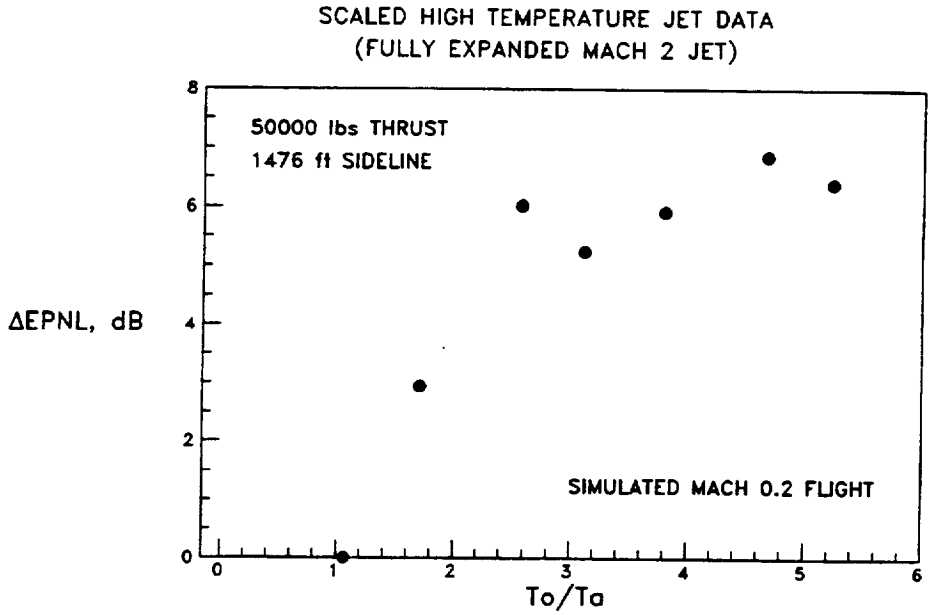

Figure 10

The results of the high temperature study of jet noise associated with the round fully pressure balanced Mach 2 nozzle, provides valuable insight of the scaled noise field for HSR applications. Figure 10 shows computed values of EPNL for several jet total temperatures, ranging from ambient to 1534°K. The EPNL values are shown relative to the near ambient jet total temperature of 313°K. The data is corrected to 50000 lbs. of thrust at a sideline distance of 1476 feet. Forward flight is simulated for M_f = 0.2 to enable the EPNL calculation. Jet noise is corrected for forward flight using standard modules found in the NASA ANOPP code (Zorumski 1982).

The EPNL metric is found to remain relatively constant, near 6 PNdB greater than the reference temperature of 313°K, for temperature ratio's greater than 2.5 (i.e. T_j = 755°K). The principle reason why the EPNL metric asymptotes with temperature is related to the generation of significant high frequency jet noise that is not weighted into the metric. Typical HSR jet total temperatures are expected to be near 1140°K for a 700 lbm./sec. engine at take-off power. In the HSR program, a mixer/ejector achieving fully mixed flow at the ejector exit with 100% pumping would have an exhaust temperature near 755°K.

From the data in figure 10, it is clear that at this temperature the same amount of noise would have to be removed as at the higher temperatures. The current reason, however, why the industry seeks lower temperatures solely rests in the observation that jet noise suppressors have thus far worked much more effectively at lower velocities (i.e. lower jet total temperatures). The pay-off is big, however, if a satisfactory scheme could be devised to achieve suppression at higher jet total temperatures. At high jet temperatures, the engine weight flow is significantly lowered to achieve the same thrust thus reducing engine size and weight. Higher jet engine temperatures also lead to more efficient engine cycles.

AXIAL DEVELOPMENT OF A SUPERSONIC JET

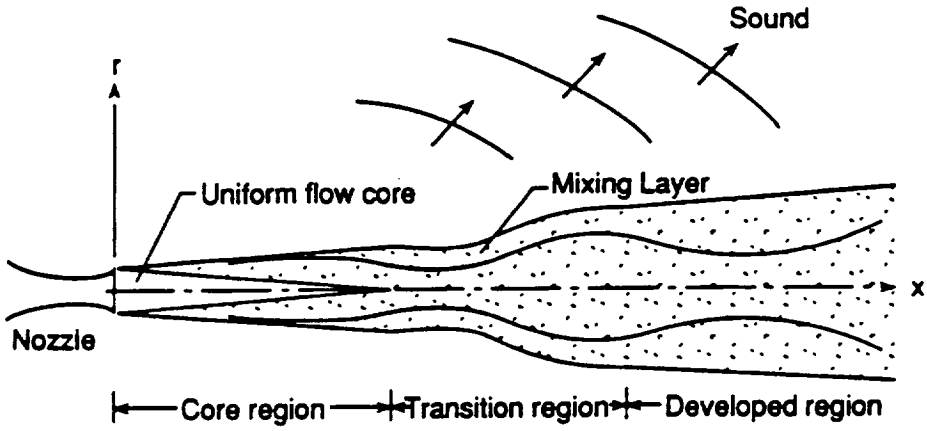

Figure 11

All free jets are divided into three main regions of flow development, as shown in figure 11. The near field region of jet development is known as the core region. In this region the initial shear grows nearly linearly with the slowest growth rate of all regions. For well designed nozzles, a nearly turbulent free region exists bounded by the inner side of the shear layer. The core region extends several jet exit diameters downstream, the axial extent being primarily a function of jet exit and free stream Mach number. For a static Mach 2 nozzle, this distance is approximately 10 diameters. In the fully developed region of jet, the flow develops in a self preserving state where mean flow variables vary like r/x. In this region the jet spreads at a greater rate than in the core region. The transition region is one where the flow adjusts between the core and fully developed region. In this region large changes occur in the turbulent structure; the Reynolds stress tensor peaks in this region. It is the rapid change in turbulent structure in this region that is the cause for the generation of the most intense noise.

JET MEAN FLOW FIELD PARAMETERS

Half-Gaussian profile parameters

- h - radius of potential core
- R - radial coordinate
- $R_{.5}$ - radius to half jet velocity
- V - axial velocity
- V_{CL} - axial centerline velocity
- V_j - fully expanded jet exit velocity

$$V / V_{CL} = 1 \qquad R \le h$$
$$V / V_{CL} = EXP(- (\ln 2)\, \eta^2) \qquad R \ge h$$
$$\eta = (R - h) / b$$
$$b = R_{.5} - h$$

Crocco's relation

$$\rho_j / \rho = (1 + .5(\gamma - 1)M_j^2)(T_A / T_o + (1 - T_A / T_o)(V / V_j)) - .5(\gamma - 1)M_j^2 (V / V_j)^2$$

Figure 12

Analysis of the noise radiated by a supersonic jet requires information concerning development of the flow in all three regions of jet flow development, although the core and transition are of most importance. Application of the compressible Rayleigh model to predict noise only requires information concerning the mean flow, whereas application of Lighthill's or Lilley's equation requires considerable information concerning the second derivative of a two point space-time turbulent Reynolds stress tensor. This paper is concerned with evaluation of the former model because of its relative simplicity and prior accuracy in prediction of important aerodynamic and acoustic physical features with low temperature supersonic jets.

The usual approach is to use a half-Gaussian profile to represent the axial mean velocity profile. This means that the Rayleigh analysis assumes that jets spread relatively slowly since the radial mean velocity is neglected relative to the axial component. This appears a satisfactory assumption for simple laboratory jets. Figure 12 shows that to establish the half-Gaussian profile in all regions of jet flow development would only require knowledge of the potential core radius, h, the radius to half jet velocity, $R_{.5}$, and the axial mean centerline velocity, V_{cl}. The jet density is then determined from jet exit operating conditions and Crocco's relation, which holds identically for isothermal jets. For the present Mach 2 jet, the flow is isothermal near a jet total temperature of 500°K.

CENTERLINE VELOCITY DECAY WITH JET TEMPERATURE
Fully Pressure Balanced Mach 2 Jet Into Still Air

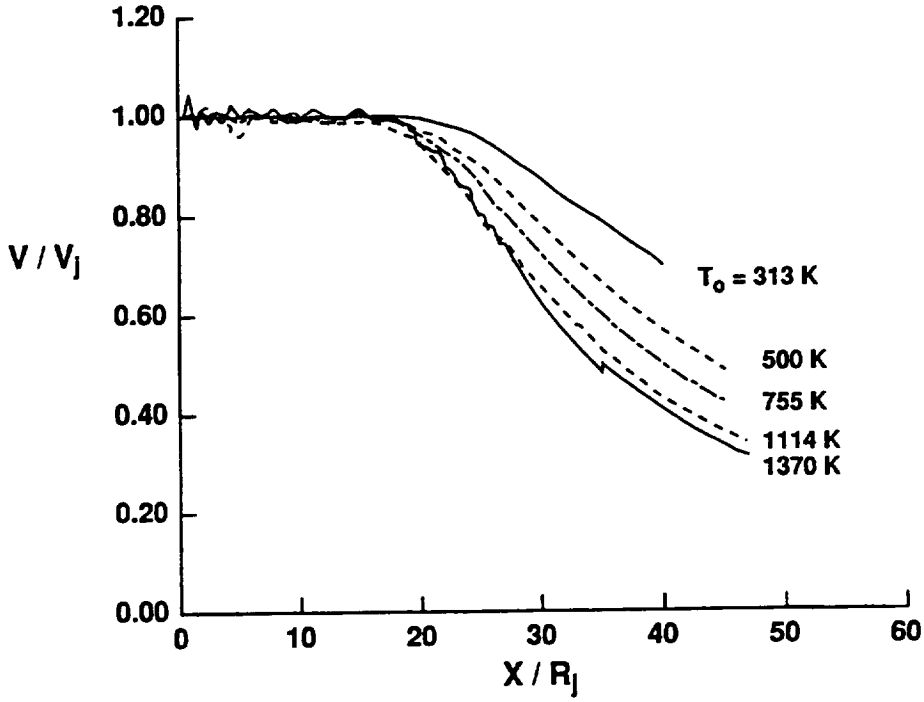

Figure 13

The experimentally determined jet centerline velocity, V_{cl}, is shown in figure 13 for several jet total temperatures ranging from 313 to 1370°K. The centerline velocity data is normalized by the jet exit velocity, which is computed from the operating pressure and temperature stagnation conditions in the nozzle plenum. The axial distance is normalized by the jet exit radius. For this data, the jet nozzle is operated fully pressure balanced and into still air.

Except for the influence of weak shocks in the jet plume, the centerline velocity for all jet total temperatures remains uniform over the first 16 jet radii from the nozzle exit. Beyond this region, the difference in velocity for the various jet temperatures increases substantially with axial distance. Examination of this data shows that the jet potential core length, L_c , generally decreases with increasing jet temperature.

Instability Wave Model - Mean Flow Profiles

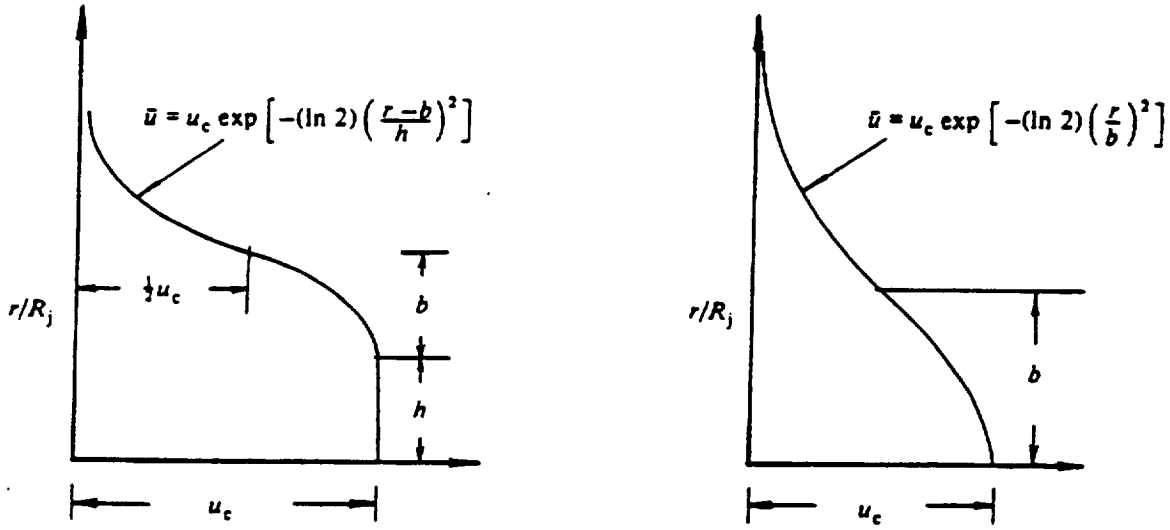

Figure 14

Figure 14 displays typical appearance of the mean velocity profiles obtained using the half-Gaussian profile for flow in the core (left side figure) and transition and fully developed regions (right side figure). Note the radius of the potential core, h = 0, beyond the core region.

TEMPERATURE DEPENDENCE ON MEASURED JET SPREAD RATE PARAMETERS

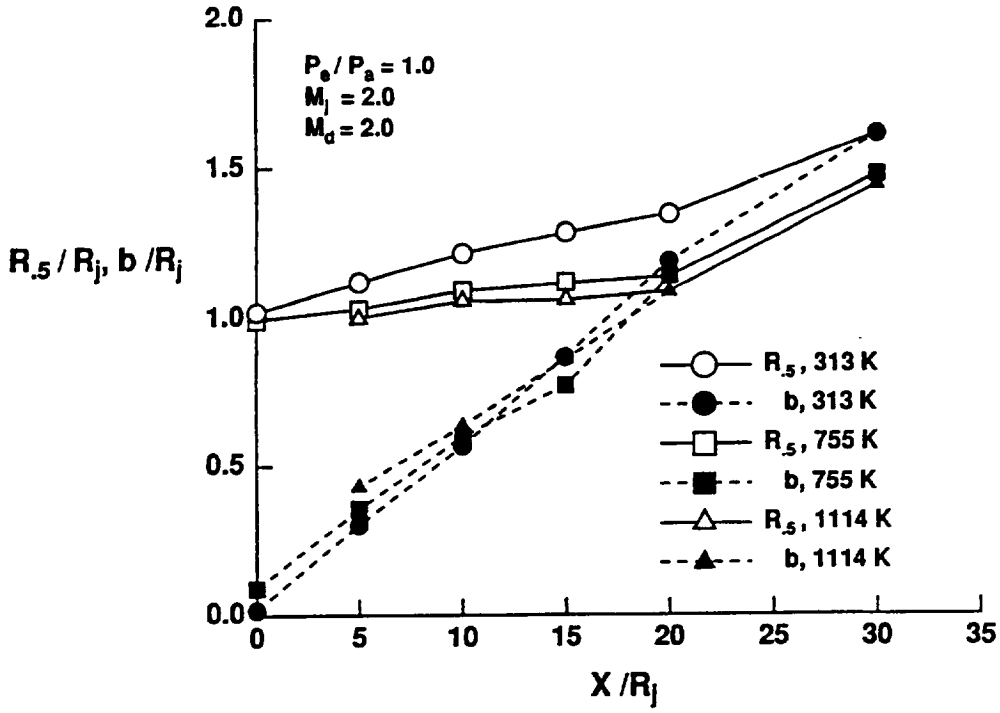

Figure 15

Figure 15 shows the measured axial variation of the radius to half velocity, $R_{.5}$, and velocity half width of the mixing layer, b, as defined in figures 12 and 14, for the three jet total temperatures of 313, 755, and 1114°K. These parameters are normalized by the nozzle exit radius. The axial development of these spread rate parameters indicates that the shear layer growth of the inner boundary toward the jet centerline is much greater for hot jets than cold jets. The outer radial boundary of the shear layer is observed to grow at a slower rate for hot jets than cold jets. The overall net result is that the potential core of hot jets is slightly reduced compared to cold jets. Figure 15 also indicates that the most significant difference in spread rate occurs between jets operating below and above isothermal jet temperatures.

RADIAL MEAN VELOCITY PROFILES

$(0.1 \leq x/D \leq 15.0)$

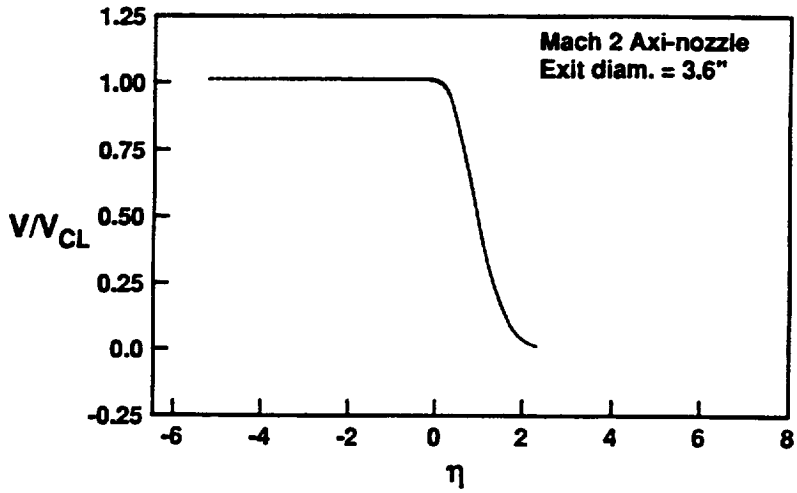

Figure 16

The universal half-Gaussian shape of the measured mean velocity profiles are shown in figure 16 for the three jet temperatures considered above. The data represents a compilation of all measured velocity profiles from the nozzle exit to 30 R_j. The data in the figure is plotted, for clarity, using lines connecting the data points. The collapse of the data points is quite good, providing a satisfactory data base for application of the Rayleigh model.

MEASURED CONVECTION MACH NUMBERS

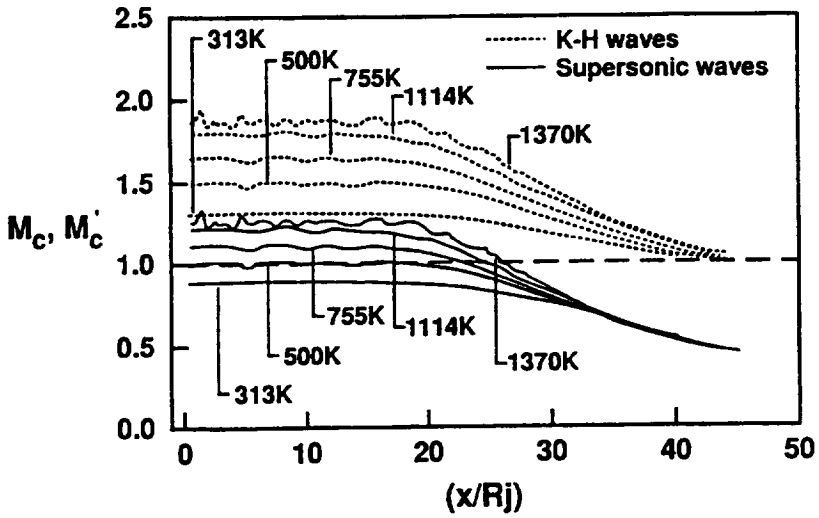

Figure 17

The Mach wave mechanism can produce noise only in those regions where a turbulent structure's phase velocity is supersonic. The phase velocities for the supersonic and Kelvin-Helmholtz instabilities are given in figure 2 in terms of their convection Mach numbers. These equations are used along with the measured properties to compute the convection Mach number for both families of instability waves. Figure 17 presents results of this analysis for all 5 jet total temperatures investigated. When either M_c or M_c' fall below unity, noise emission by the Mach wave process is terminated.

The data in figure 17 show that supersonic phase velocities for supersonic instability waves do not extend far beyond the end of the potential core. On the other hand, the phase velocity for the Kelvin-Helmholtz (K-H) instabilities are supersonic well beyond the end of the potential core. The axial extent of the noise producing region for this second family of waves is thus quite extensive. The K-H waves have supersonic phase speed to near $X/R_j = 46$, independent of the jet total temperature. Thus the axial region for noise emission by the Mach wave emission mechanism does not appear to increase with jet total temperature.

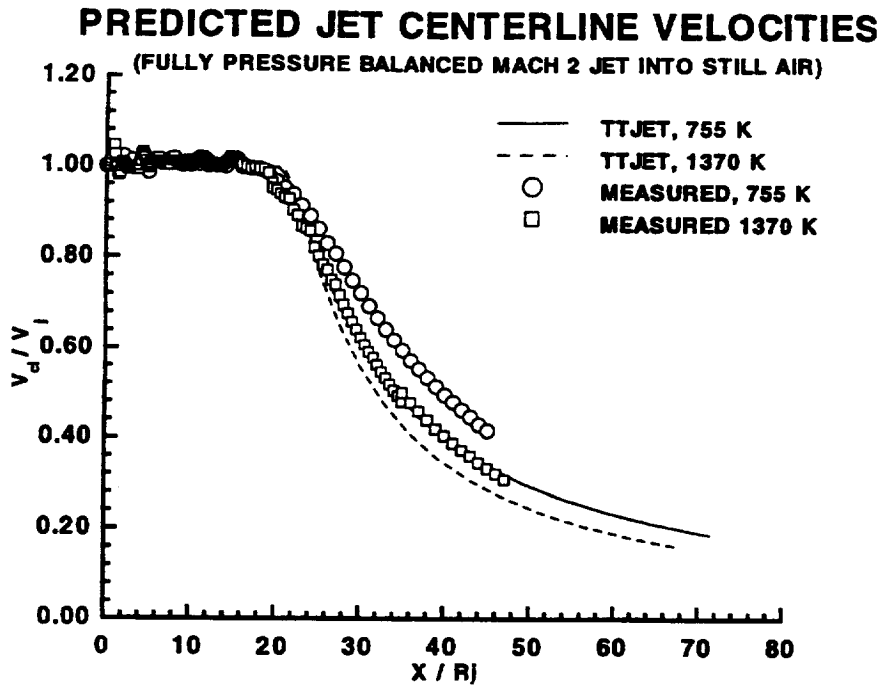

Figure 18

In figure 18, comparison is made between the SAIC TTJET code prediction of Dash and Kenzakowski (1992) for centerline velocity and the measured data for jet total temperatures of 755°K and 1370°K. The TTJET code is a parabolized Navier-Stokes solver with up-wind differencing. and Pope (1978) centerline corrections for vortex stretching. It utilizes a two equation turbulence model with compressibility corrections based on the work of Sarkar, Erlebacher, Hussani, and Kreiss (1989). The predicted potential core length is slightly greater than measured values. When T_o = 755°K the measured and predicted values for L_c are respectively 18.25 R_j and 20.51 R_j. When T_o = 1370°K the respective measured and predicted values are 18.83 R_j and 20.85 R_j.

Beyond the potential core, deviations between the predicted and measured values become more apparent. The predicted jet centerline velocities decay much faster than do measured data. The measured data indicates that differences in centerline velocity decay with temperature are greater than those predicted. The observed differences between measured and predicted centerline data suggest that the TTJET code predicts much greater mixing in this downstream region. This behavior could be attributed to performance of the compressible turbulence dissipation model installed in the code.

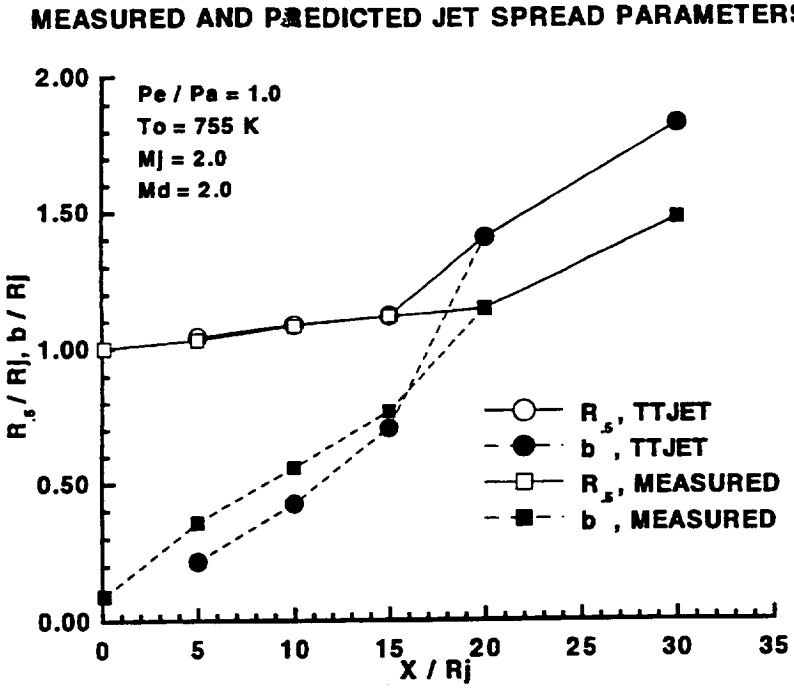

Figure 19

In figure 19, a comparison is made between the measured and TTJET code predictions for $R_{.5}$. These appear to be in outstanding agreement with measured values. However, the specification of a 10% initial boundary layer thickness in the code calculations overestimates the real nozzle exit boundary layer thickness. Thus the numerical jet appears to have a thicker shear layer thickness to $X/R_j = 15$. Beyond this point, the TTJET code predicts substantially greater mixing than observed experimentally.

It is well known from previous experimental studies that beyond the potential core region the turbulence structure must respond to a rapid transition of the mean flow from annular to axisymmetric shape. The large scale turbulence structure generally transitions from helical to axisymmetric spatial structure. The kε-CD turbulence model does not contain the methodology to accommodate these flow field characteristics. The quantitative difference between the predicted and measured jet spread rate parameters is expected to play an important role in application of the compressible Rayleigh equation. The major noise producing region occurs near the end of the potential core, where the most highly amplified instability wave reaches its maximum growth. This growth is strongly dependent upon representation of the mean flow field. The accelerated rapid mixing of the numerical predictions near the end of the potential core would produce, based on application of the Rayleigh model, slightly lower values for noise if based on mean flow data predicted by the TTJET code.

PREDICTED CONVECTION MACH NUMBERS

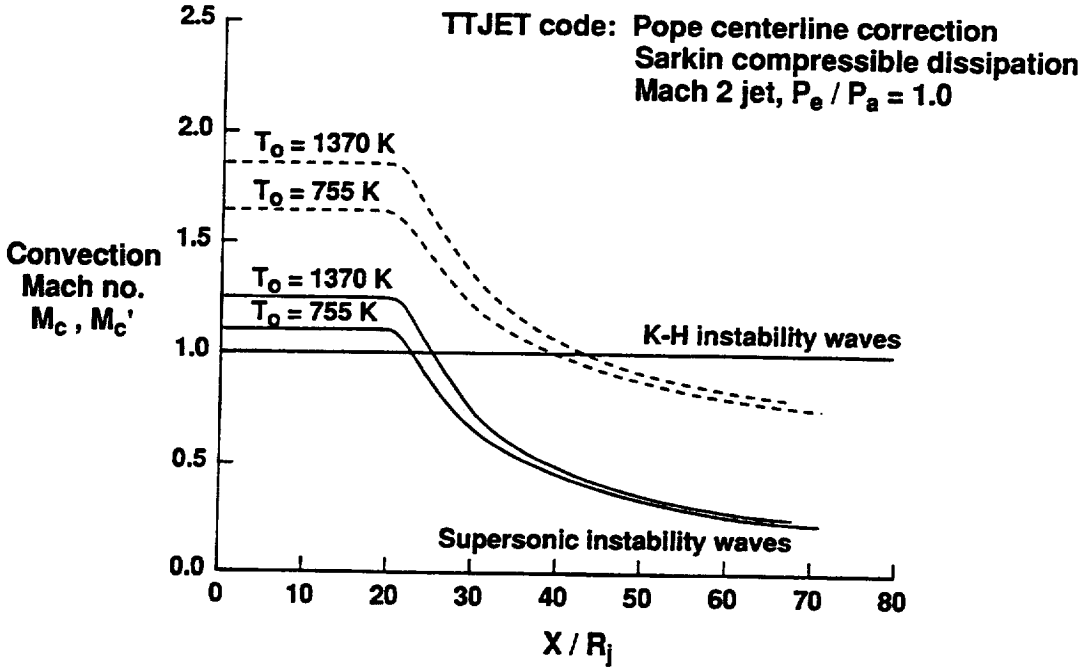

Figure 20

The TTJET code predictions for the convection Mach numbers of the supersonic and Kelvin-Helmholtz (K-H) instability waves are shown in figure 20 for the jet total temperatures of 755°K and 1370°K. The predicted values for M_c and M_c' provide essentially the same information as the experimentally determined values. The TTJET code predicts supersonic phase speeds for the K-H wave to $X/R_j = 42$. This decreased distance, relative to the experimentally determined values in figure 17, is consistent with the more rapid mixing of the numerically simulated jet.

Instability Wave Model

- Compressible Rayleigh's Equation

$$\frac{\partial^2 \hat{p}}{\partial r^2} + \frac{\partial \hat{p}}{\partial r}\left[\frac{2\alpha}{\Omega}\frac{\partial U}{\partial r} + \frac{1}{r} - \frac{1}{\bar{\rho}}\frac{\partial \bar{\rho}}{\partial r}\right] + \left[\bar{\rho}M_j^2\Omega^2 - \frac{n^2}{r^2} - \alpha^2\right]\hat{p} = 0$$

$$p(r,\theta,x,t) = A(x)\hat{p}(r)\exp\left[i(\alpha x + n\theta - \omega t)\right]$$

$$\alpha = \alpha_r + i\alpha_i \qquad c = \frac{\omega}{\alpha_r}$$

Figure 21

Linear instability wave theory for supersonic jets is now well-known. It can be shown that development of an instability wave of fixed real frequency, ω, is governed by the compressible Rayleigh equation shown in figure 21 in the top equation, where $\Omega = \omega - \alpha U$. Here U and ρ are the mean velocity and density, respectively, and M_j is the fully expanded jet Mach number. The parameter, n, is the azimuthal mode number and α is the axial wavenumber or eigenvalue of the problem. The equation is written in a cylindrical polar coordinate system (r,ϕ,x) with the jet axis aligned with the x-direction. Here, it is assumed that the flow is locally parallel and that fluctuating pressure can be written as in the second expression, where A(x) is the amplitude function. The axial wavenumber, α, is complex as shown, where α_i controls the growth rate and α_r determines the phase speed as shown.

Instability Wave Model - Numerical Scheme

- Set up the Inner & Outer Solutions
- Integrate Numerically in the Shear Layer
  - variable step-size Runge-Kutta algorithm
- Match Solutions at the Intermediate Point

$$\hat{p}_I\hat{p}'_o - \hat{p}'_I\hat{p}_o = \Delta(\omega, \alpha) = 0$$

- Newton-Raphson Iterative Scheme

Figure 22

The procedure used to solve the Rayleigh equation is shown in figure 22. The usual procedure, as indicated, is to formulate the solution as an eigenvalue problem. Here, α, is the unknown eigenvalue, which for a fixed real frequency ω is determined iteratively using a Newton-Raphson scheme. The inner and outer shear layer pressure amplitude functions are determined by intregrating numerically through the shear layer using a variable step-size Runge-Kutta algorithm from both the outer and inner directions and matching an intermediate point.

Instability Wave Model - Inner & Outer Solution

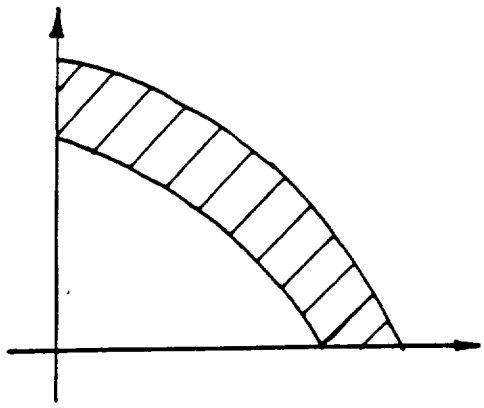

$$\hat{p}(r) = J_n(i\lambda_i r), \lambda_i(\alpha) = \left[\alpha^2 - M_j^2(\omega - \alpha U)^2\right]^{\frac{1}{2}}$$

$$\hat{p}(r) = H_n^{(1)}(i\lambda_o r), \lambda_o(\alpha) = \left[\alpha^2 - \bar{\rho}_\infty M_j^2 \omega^2\right]^{\frac{1}{2}}$$

Figure 23

Figure 23 shows the forms assumed for the instability wave's pressure. These eigenfunctions are consistent with the cylindrical polar coordinate system used in the Rayleigh equation. The upper equation is associated with the inner shear layer, which satisfies boundary conditions associated with the boundedness condition at r = 0. The lower equation is associated with the outer boundary, which satisfies boundary conditions associated with outgoing waves.

Instability Wave Model - Far Field Directivity

$$p(r,\theta,x,t) = \int_{-\infty}^{\infty} g(k) H_n^{(1)}(i\lambda_k r)\exp\left[i(kx + n\theta - \omega t)\right] dk$$

$$\lambda_k = \left[k^2 - \bar{\rho}_\infty M_j^2 \omega^2\right]^{\frac{1}{2}}$$

$$A(x) = A_o(x_o)\exp\left[\int_{x_o}^{x}(i\alpha_r - \alpha_i)dx\right]$$

$$g(k) = \frac{1}{2\pi}\int_{-\infty}^{\infty} A(x)\exp(-ikx)dx$$

$$D(\chi) = \lim_{R\to\infty}\frac{1}{2}R^2 \mid p \mid^2 = 2 \mid g(\bar{\rho}_\infty^{\frac{1}{2}} M_j \omega \cos\chi) \mid$$

Figure 24

Following the procedure of Tam and Burton (1984) of matching the inner and outer solutions, the acoustic pressure, p(r,θ,x,t), in the region outside the jet flow is given by the first equation in figure 24, where the second equation defines the eigenvalue λ_k. The streamwise variation in amplitude and phase of the instability wave, A(x), is given by the third equation. The wavenumber spectrum, g(k), is obtained from the Fourier transform A(x) as indicated in the fourth equation. The farfeild directivity function, D(x), defined as the sound power radiated in a direction per unit solid angle by an instability wave of frequency ω, is given in the bottom equation.

Modes of Instability

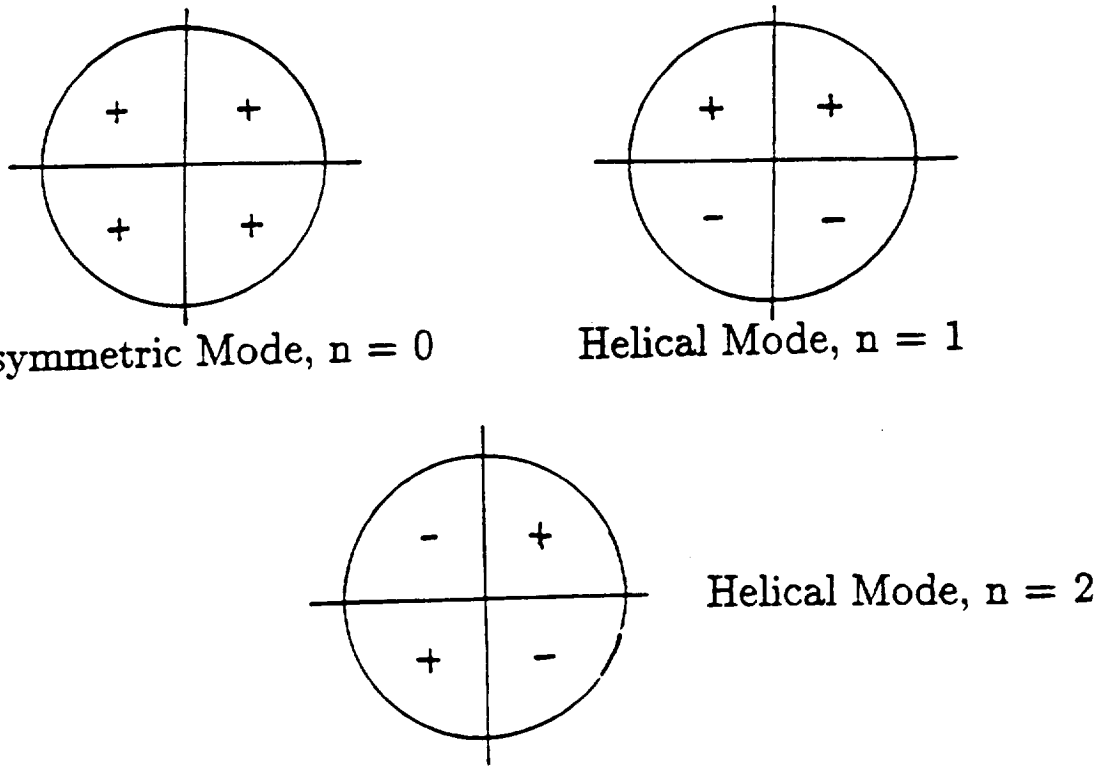

Figure 25

Figure 25 provides several examples of the instantaneous instability wave pressure in a cross plane associated with the first few fundamental modes n = 0, 1, and 2. These modes are generally considered the most dominant modes of instability, in that they are generally the most highly amplified instability waves in a cylindrical shear layer with a half-Gaussian mean velocity profile.

Modes of Instability

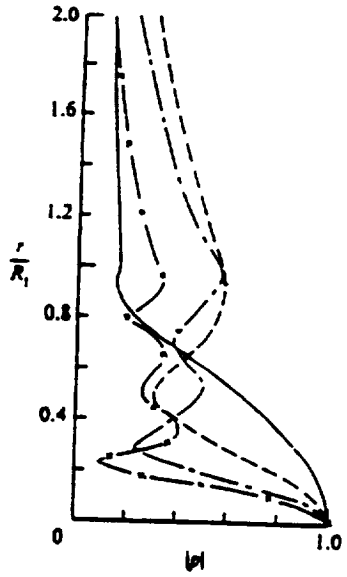

Supersonic Instability Wave. —, (0,1) Mode; – – –, (0,2) Mode; – – –, (0,3) Mode; –x–x–, (0,4) Mode

Figure 26

In figure 26 example radial distributions are shown for the first few elementary supersonic instability wave pressure fields. Even though calculations were performed for jet total temperatures to 1370°K, only the (0,1) mode achieved supersonic phase speed. Thus only this mode would radiate sound to the far field. Higher jet temperatures, however, would be expected to produce higher order supersonic instability waves with supersonic phase speed.

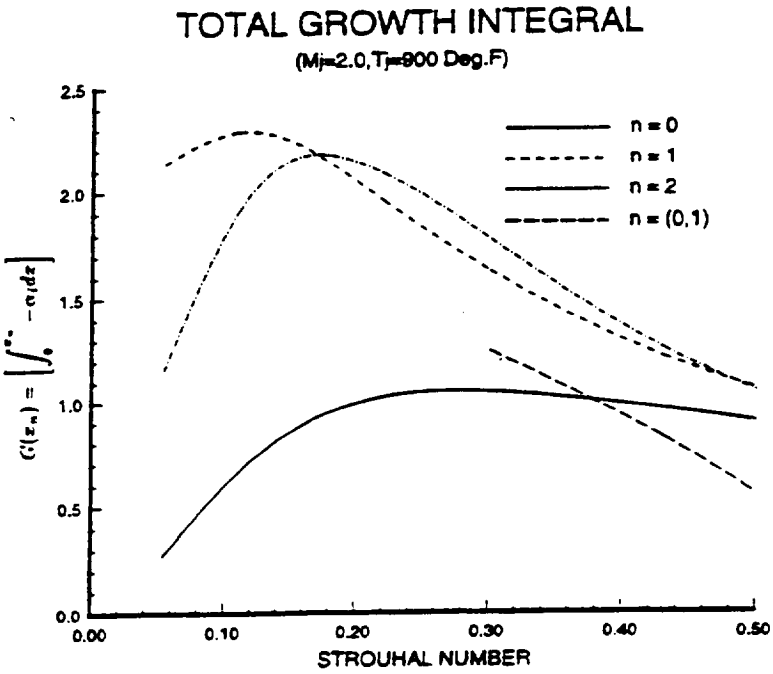

Figure 27

Instability wave theory suggests that noise characteristics of hot supersonic jets in the peak radiation direction are related to those of the most highly amplified instability wave. The total amplification of an instability wave of frequency, ω, and mode number, n, is related to the growth rate of the wave, which is functionally related to the sign and magnitude of α_i, the imaginary part of the axial wavenumber α. The total growth integral, evaluated to a wave's neutral point x_n (i.e. $\alpha_i = 0$), is used as a gauge for the relative importance of a given mode at a specified frequency to produce noise. The total growth integral is plotted as a function of Strouhal number in figure 27 for several K-H modes and the one supersonic instability wave with supersonic phase speed. From figure 27 it can be noted that the axisymmetric K-H wave is relatively unimportant over the entire Strouhal range shown. The same applies to the supersonic instability wave, where supersonic phase speeds were obtained only for Strouhal numbers above 0.3. Both the first and second order helical modes achieve the highest growth rates. In the Strouhal number range for maximum noise emission, $0.05 \leq S_t \leq 0.1$, the first order helical dominates. In the Strouhal number range above 0.1, both first and second order helical modes are equally important. This suggests that one should, in the future, consider even higher order modes for hot jets.

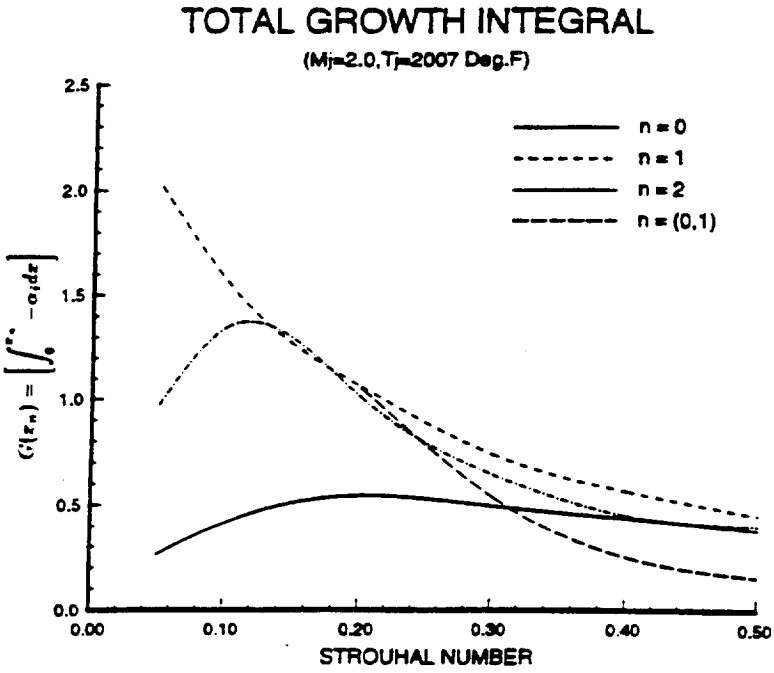

Figure 28

In a similar fashion, the total growth integral results for the jet total temperature of 1370°K is shown in figure 28. Immediately apparent is the increased significance of the supersonic instability wave, which is now competitive with the K-H waves in the Strouhal number range above 0.2. Again the first order helical mode dominates the Strouhal number range associated with peak noise emission, although all amplitudes for K-H waves have diminished from those computed for the previous 755°K jet temperature. The axisymmetric mode only achieves importance in the higher Strouhal number range above 0.3. The fact that all modes calculated have nearly identical importance at higher Strouhal number represents a major difficulty in application of the Rayleigh model. The utility of the Rayleigh model diminishes when many modes become significant, since the present theory cannot assign initial amplitudes to any of the modes. In the present calculations, it is assumed that all modes have equal initial amplitudes. This is a restrictive assumption, since in reality one expects the initial shear layer receptivity to disturbances to be dependent on wave frequency and mode number.

STROUHAL DEPENDENCE WITH JET ANGLE
Spectrum Level Data, 12 ft. Circular Arc

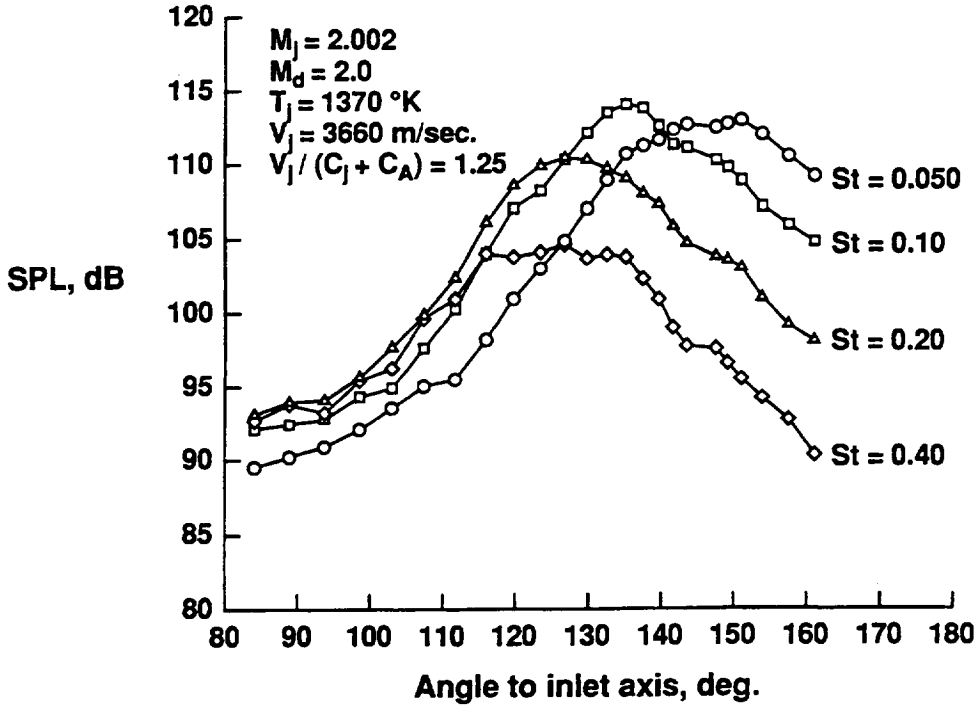

Figure 29

The angular dependence of the Strouhal frequency is important in verification of the application of spatial stability theory to solve the compressible Rayleigh equation for prediction of noise emission. Figure 29 shows this dependence for the major Strouhal frequencies of interest at 1370°K. The data is normalized by the spectral amplitude corresponding to the maximum value, P_o, among all four Strouhal frequency components. This normalization procedure is chosen since instability wave theory cannot predict absolute values for noise radiation. As can be observed, the S_t = 0.05 and 0.01 components are dominant frequencies, but peak at different angles to the inlet axis. The 0.4 component is least significant and has a peak amplitude 10 dB less than the 0.1 component. Recalling figure 7, the Mach wave emission process peak is only 15 dB above what may be considered noise generated by small scale turbulence. Thus the 0.4 component directional amplitude characteristics shown in figure 29 may be influenced by noise generated by small scale turbulence.

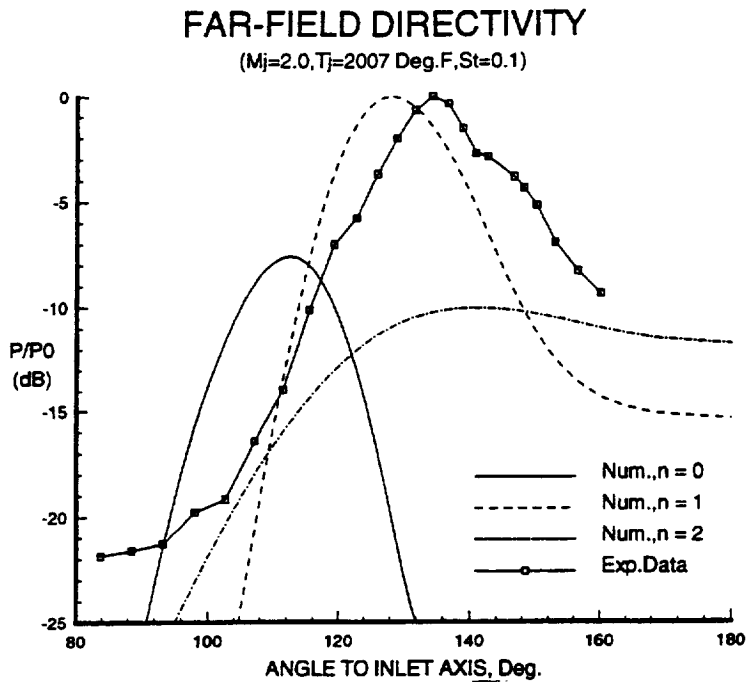

Figure 30

Figure 30 shows a comparison between the measured directivity of the 0.1 Strouhal frequency component and the Rayleigh prediction of noise for the three K-H waves n = 0, 1,2. The jet total temperature is 1370°K, but for this Strouhal frequency there is no solution for a supersonic instability wave. The predicted far field pressure for each of the instability modes is normalized using the same procedure provided in figure 29. All K-H waves are initialized with equal amplitudes at the nozzle exit. From this comparison, it is apparent that the first order helical mode is the most dominant component. Both the axisymmetric mode, n = 0, and the second order helical mode, n = 2, contribute equal amounts to the sound field. Note that the data shows inflections near those angular positions where each respective mode achieves their peak amplitude. The angular shift between data and computation is related to the finite distance the data was collected from the nozzle (R = 12 ft.). Adjustment for true source location in the jet would shift all measured data several degrees toward the numerically predicted data.

PREDICTION OF FAR FIELD DIRECTIVITY FOR S_t = 0.4

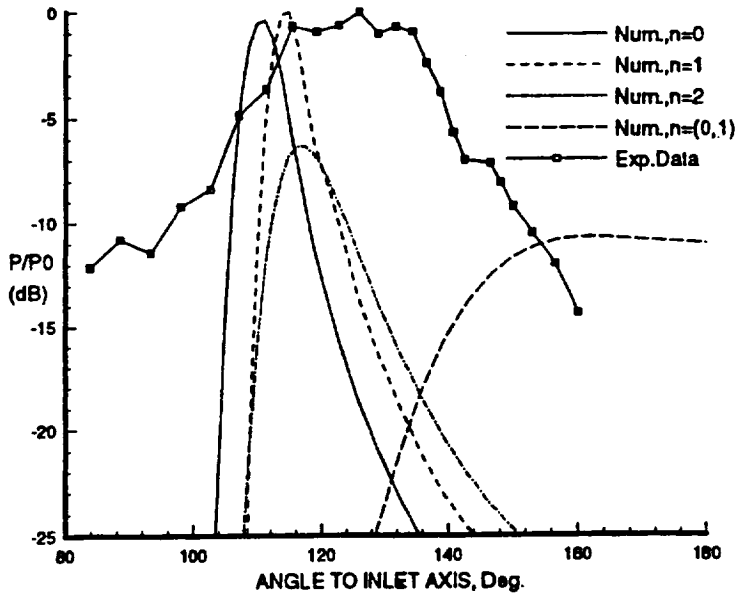

Figure 31

Figure 31 shows a similar comparison between predicted and measured acoustic data for the 0.4 Strouhal frequency component. Here we see that both the axisymmetric and first helical K-H wave is equally important. One also sees that the (0,1) mode supersonic instability wave has a direct influence on the predicted noise radiation at narrow angles to the jet axis. The measured data also shows signs of its existence. In general we see that the comparison to data is not as good as that obtained at lower Strouhal number. This may be due to the influence of noise generated by fine scale turbulence.

NOISE REDUCTION ASSOCIATED WITH HOT NON-ROUND JET EXIT GEOMETRY

1160°R jet temp; constant thrust/ mass flow comparison

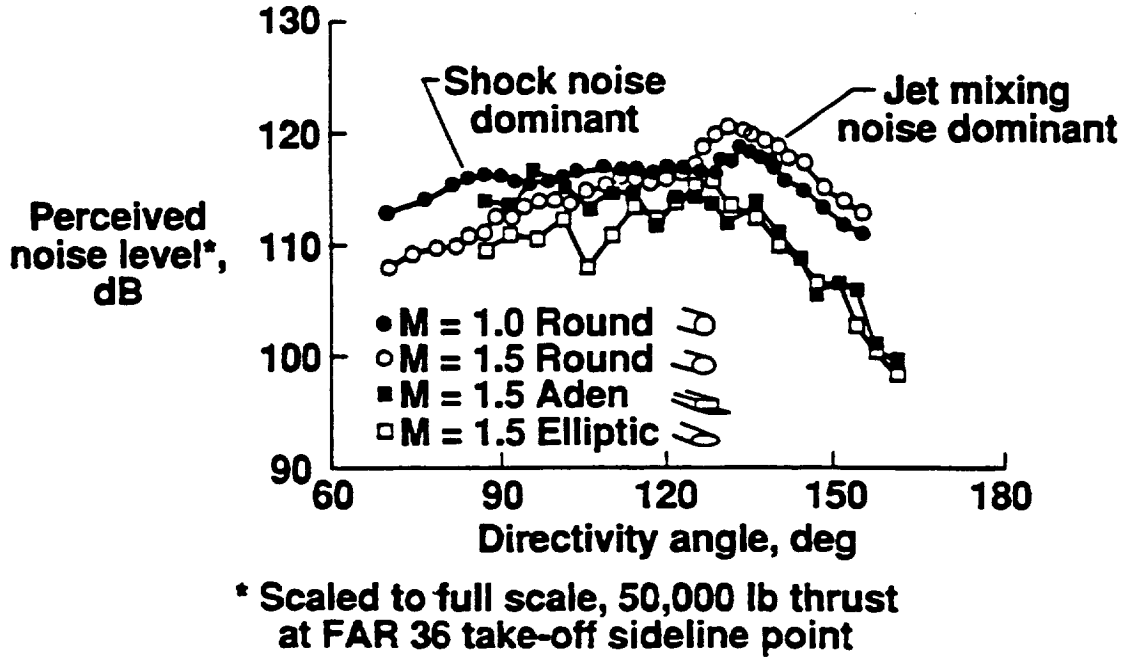

* Scaled to full scale, 50,000 lb thrust at FAR 36 take-off sideline point

Figure 32

A study was recently conducted to determine the noise reduction potential associated with simple single nozzle ducts of various geometries. Figure 32 shows a comparison of noise emitted by a round convergent nozzle, a round convergent-divergent nozzle with exit design Mach number of 1.5, an elliptic convergent-divergent nozzle with an aspect ratio of 2 and design Mach number of 1.5, and an Aden nozzle (i.e. rectangular geometry) with an aspect ratio of 2 and design Mach number of 1.5. The data is presented in terms of perceived noise level in dB as a function of angle to the nozzle inlet axis. The jet temperature for all nozzles was 1160°R and the data has been normalized to 50,000 pounds of thrust at the FAR 36 sideline distance of 1476 feet. As is evident both the elliptic and Aden nozzles produce significant noise reduction in the peak noise direction, $\psi \geq 120°$. However, unlike the Aden nozzle, the elliptic nozzle has very low levels of shock noise, so that significant reductions are obtained at all angles to the jet axis. The single elliptic nozzle produces a noise reduction between 7 and 8 PNdB relative to the baseline convergent nozzle.

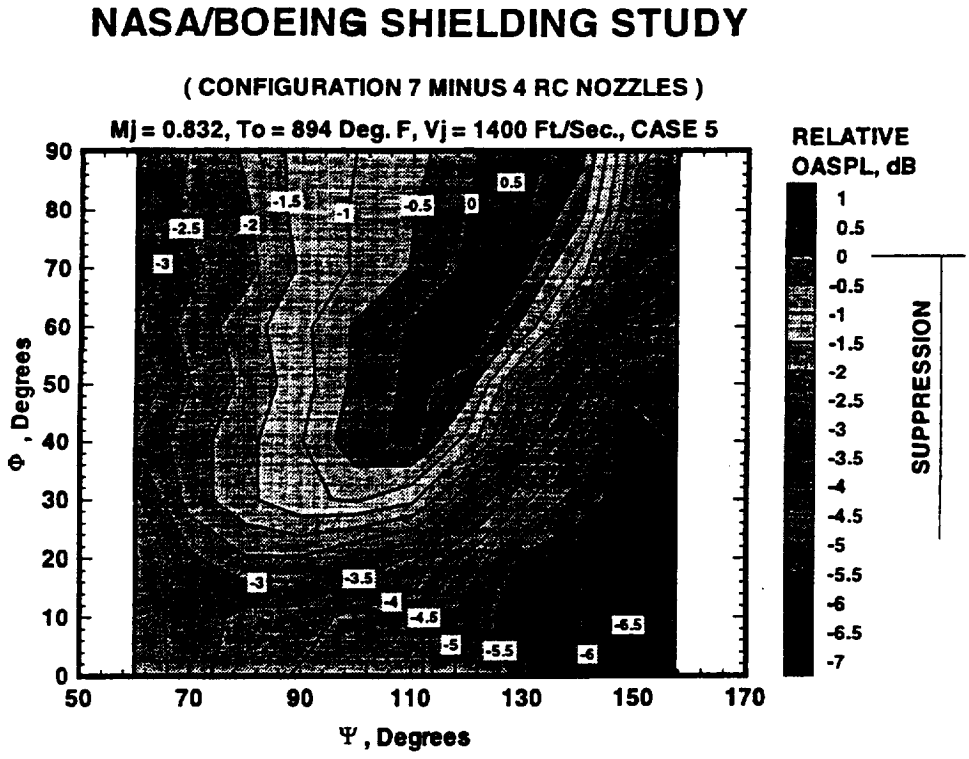

Figure 33

Figure 33 shows a comparison between noise emitted by 4 interacting in line nozzles and 4 non-interacting equivalent baseline round convergent nozzles. The 4 interacting nozzles are separated by 2.5 jet exit diameters. The noise produced by the 4 non-interacting jets is computed from ANOPP with each synthetic nozzle located at the equivalent location of the 4 interacting nozzle locations. The contour map of figure 33 shows the result of substracting the non-interacting jets from the measured noise of the interacting jets. At $\Phi = 0°$, the azimuthal view is sideline along the axis joining all nozzles. At $\Phi = 90°$, the azimuthal view is normal to the plane containing the four nozzles. It can be observed that significant noise reductions occur in the sideline direction. At $\Phi = 0°$ and $\Psi = 150°$, the 6 dB relative noise reduction indicates complete shielding of noise by the near jet of all other noise generated by the remaining nozzles. At $\Phi = 90°$ and $\Psi = 90°$, the -1.5 dB relative noise reduction indicated that aerodynamic interaction of the jet plumes may have led to faster decay of jet centerline velocity and thus lower noise. Only a small region exhibits a slight noise increase at $\Phi = 90°$ and $\Psi = 130°$.

REFERENCES

Dash, S.M., and Kenzakowski, D.C., 1992, Private Communication.

Oertel, H., 1982, "Measured Velocity Fluctuations Inside the Mixing layer of a Supersonic Jet", Recent Contributions to Fluid Mechanics, Berlin, Springer Verlag, pp. 170-179.

Pope, S.B., 1978, "An Explanation of the Turbulent Round-Jet/Plume-Jet Anomaly, AIAA J., March, pp. 279-281.

Sarkar, S., Erlebacher, G., Hussaini, M.Y., and Kreiss, H.O., "The Analysis and Modeling of Dilitational Terms in Compressible Turbulence", ICASE Report No. 89-79.

Seiner, J.M., Ponton, M.K., Jansen, B.J., and Lagen, N.T., 1992, "The Effects of Temperature on Supersonic Jet noise Emission", DGLR/AIAA 92-02-046.

Tam, C.K.W. and Burton, D.E., 1984, "Sound Generated by Instability Waves of Supersonic Jets, Part 2, Axisymmetric Jets", J. Fluid Mech.., Vol. 138, pp. 273-295.

Tam, C.K.W. and Hu, F.Q., 1989, "On Three Famlies of Instability Waves of High Speed Jets", J. Fluid Mech., Vol. 201, pp. 447-483.

Zorumski, W.E., 1982, "Aircraft Noise Prediction Program Theoretical Manual", NASA TM 83199.